Environmental Earth Sciences (2021) 80:105
https://doi.org/10.1007/s12665-021-09391-2

THEMATIC ISSUE

The origin of gley colors in hydromorphic vertisols: the study case of the coastal plain of the Río de la Plata estuary

Mauro Gómez Samus[1] · Marcos Comerio[2] · María Luciana Montes[3] · Laura Boff[4] · Julia Löffler[5] · Roberto Carlos Mercader[3] · Juan Carlos Bidegain[6]

Received: 29 February 2020 / Accepted: 14 January 2021

Abstract

This work aims to contribute to the interpretation of soil colors; mainly to identify the pigments that generate the greenish colors in hydromorphic conditions (gley colors) in vertisols of the coastal plain of the Río de la Plata estuary. These colors are of cold hues, generally greenish (olive-gray), and occur in poorly drained soils with prolonged water accumulation. For this purpose, samples of Bssg horizons of hydromorphic vertisols from the coastal plain of the Río de la Plata estuary were analyzed using routine and chemical analyses, Mössbauer spectroscopy, determination of rocks magnetic parameters, X-ray diffraction, thermogravimetric and differential thermal analysis and petrographic-electronic microscopy. The pigments associated with the gley colors of these soils are mainly due to ferric iron content, corresponding to minerals such as ferric iron-rich smectites (nontronite/Fe-rich beidellite) and oxy-hydroxides like goethite, which colors range from green to yellow. These minerals, combined with gray or black components, e.g., manganese compounds and/or organic matter, contribute to the generation of the usual gley colors in the analyzed soils of the Pampean plain. The obtained data allows us to state that it is a mistake to assing the olive color in hydromorphic soils to the presence of ferrous iron compounds, as it is traditionally done. The oxidizing condition of iron is dominant in all the analyzed samples, integrating the composition of ferric iron-rich clay minerals and oxy-hydroxides (goethite).

Keywords Vertisol · Gleysol · Stagnosol · Goethite · Nontronite · Beidellite

Introduction

The color is one of the most relevant morphological properties in the study of soils (Nickerson et al. 1945). Thus, it is a property included in the list of obligatory procedures for the description of soils in international classifications, such as WRB (IUSS Working Group WRB, 2006, 2014) and USDA-Soil Taxonomy (Soil Survey Staff 2014a). The determination of color in soils is relevant to study their environmental conditions as well as to interpret the processes involved in their formation. Consequently, it is a parameter of taxonomical relevance.

The color of soils can be a property inherited or acquired during pedogenesis (Gaucher 1971). Humus contributes strongly to the soil pigmentation, making it darker (melanization process), while oxides and oxy-hydroxides of ferric iron provide a wide spectrum of colors varying from red to yellow (rubefaction, lutefaction) (Gaucher 1971; Cornell and Schwertmann 1996). Calcic carbonates or sulfates provide whitish colors (leucinization), while the manganese oxide

This article is a part of the Topical Collection in Environmental Earth Sciences on "Advances in Environmental Geochemistry" guest edited by Dr. Eleanor Carol, Dr. Lucia Santucci and Dr. Lia Botto.

✉ Mauro Gómez Samus
mlgomezsamus@untdf.edu.ar

1 ICPA-UNTDF, Fuegia Basket no 251, Ushuaia, Argentina

2 YTEC-CONICET, Ensenada, Argentina

3 Departamento de Física, Facultad de Ciencias Exactas, UNLP, Instituto de Física La Plata (UNLP-CONICET-CCT La Plata), La Plata, Argentina

4 Instituto de Geomorfología y Suelos (IGS-UNLP), La Plata, Argentina

5 Universidad Nacional de La Plata, La Plata, Argentina

6 Laboratorio Entrenamiento Multidisciplinario para la Investigación Tecnologica (LEMIT-CIC), La Plata, Argentina

Published online: 29 January 2021

contributes to melanization (Gaucher 1971; Schulze et al. 1993). Traditionally, the color of soils has also been related to the oxidation state of iron compounds. In this sense it should be mentioned the work of Daniels et al. (1961), which considers that the greenish to bluish colors are due to the presence of ferrous iron.

Greenish colors (olive—gray) of hue 2.5Y and 5Y are included between the so-called "gleyic properties" (IUSS Working Group WRB, 2014). Originally the word "gley" was used to refer to pedologenetic materials gray to greenish colors and related to waterlogged conditions (Vysotskiy 1905). Gleyic properties (also known as gley pattern; IUSS Working Group WRB 2006) refer to materials that were under reducing conditions by an ascendant reducing agent such as ground water table for a long time. The criteria to recognize these properties are a) greenish, bluish or grayish dominant colors (reductimorphic colors), b) red color should not be over 2.5Y in Munsell system, and/or c) abundant iron/manganese mottles. These characteristics are similar to the so-called stagnic properties, where the reducing conditions are linked to a descending reducing agent (stagnation of surface water), and where abundant mottles, iron and manganese concretions, and/or greenish, bluish or light gray colors are observed (IUSS Working Group WRB, 2006, 2014).

Gleyic colors may appear, as well as stagnic properties, on practically all WRB soil groups, although they are distinctive of specific groups, such as gleysols and stagnosols. On the other hand, the United States of America classification (Soil Survey Staff 2014a) indicates that these properties are associated with soils in aquic moisture regimes (endosaturation or episaturation) in subgrups such as Aquerts, Aqualfs, Aquults, Aquents, and Aquepts, among others.

The present contribution refers to gleying as the general appearance of those soils with cold hue colors, generated under deficient drainage and long periods of water stagnation due to a rise of water table or superficial ponding. These conditions are usually closely related to those of hydromorphic soils (Thorp and Smith 1949).

Concerning the origin of the pigments giving rise to the greenish colors in hydromorphic soils (gley colors), many proposals must be taken into account. The traditional explanation relates them to the presence of ferrous iron compounds (Daniels et al. 1961; Gaucher 1971; Retallack 2001), including the green rust that belongs to a complex variety of ferrous and ferric iron hydroxides, with anions such as Cl^-, CO_3^{2-} or SO_4^{2-}, among others (Cornell and Schwertmann 2003). The ferrous iron phosphate, called vivianite, was also proposed as a generator of the greenish colors (Imbellone et al. 2010). However, other authors indicated that the presence of ferrous iron is not strictly required for the generation of these colors. Zaidelman and Nikiforova (1994) stated that it could be related to the wash out of the non-compensated iron in anaerobic conditions. Which was previously analyzed in detail by Vepraskas and Wilding (1983a, b), the later work states the cold hue color is controlled by silicate particles, without stain of ferric iron oxide or hydroxide**.** Bidegain et al. (2005) working with rock magnetic parameters of Pampean loess (La Plata, Argentina), found a total decay in the ferrous iron concentration in gley horizons. Bartel et al. (2005) mentioned the neoformation of more oxidized compounds such as hematite or goethite in waterlogged soils in one study carried out in argiudols. Besides, Vodyanitskii et al. (2005) stated that it is possible that hydromorphic environments facilitate the formation of hydrated species, such as goethite (brownish to yellow). This would be done at the expense of anhydrous oxide such as hematite, characterized by its relatively high capacity to stain sediments and soils with the reddish color. According to the obtained data, the cold hues are due to a decrease of the red stain and increase in the yellow component.

Aiming to contribute to the knowledge of the origin of gley color in waterlogged soils as well as to better understanding the processes involved, several characteristic soils of the coastal plain of Rio de la Plata estuary (Argentina) were analyzed. All the techniques were focused in determining the oxidation degree of iron and its relationship with the color of soils. The techniques applied were chemical analysis, Mössbauer spectroscopy, measurements of magnetic parameters, X-ray diffraction, differential gravimetrical thermal analysis, and optical-electron microscopy; they were analyzed together to understand the role of iron in the generation of gley colors.

Materials and methods

Soil samples

The analyzed soils, from the coastal plain in the Río de la Plata estuary in Buenos Aires province (Argentina) were taken from a topographic low (below 5 m) (Fig. 1). They correspond to hydromorphic vertisols, classified by Soil Taxonomy as Aquerts (Cappannini and Mauriño 1966; Giménez et al. 2005; Imbellone et al. 2009; Imbellone and Mormeneo 2011). These soils are poorly developed, with clayey texture but with no evidence of clay downward movement by pedogenesis (argilluviation). The sequence of horizons is frequently of the type A-Bssg1-Bssg2 (Fig. 2a). Imbellone and Mormeneo (2011) indicated intense hydromorphism, with frequent water logging and water table close to the ground level, providing episaturation and endosaturation conditions depending on annual stations. They also have a great variety of redoximorphic features, mainly low hue (hue of 2.5Y and 5Y); and chroma equal or less than 2 and presence of Fe–Mn mottled and concretions mainly concentrated in the top of the profile (in the contact zone between A and

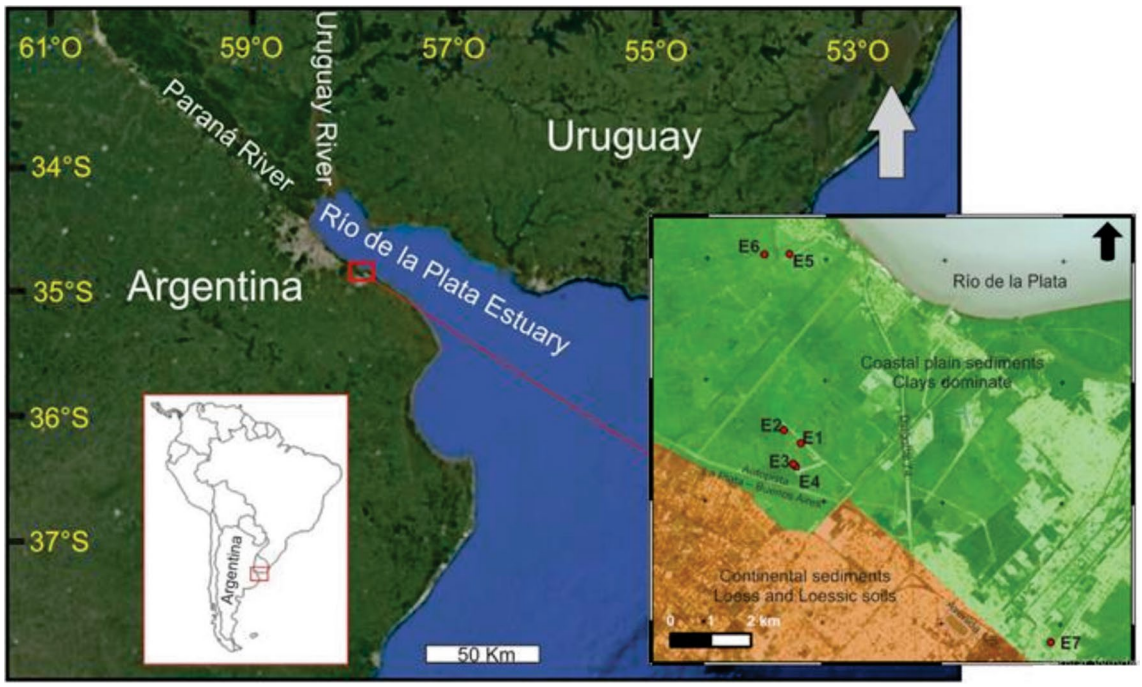

Fig. 1 Area of Study and Detail of sampled area showing the location of the test pits

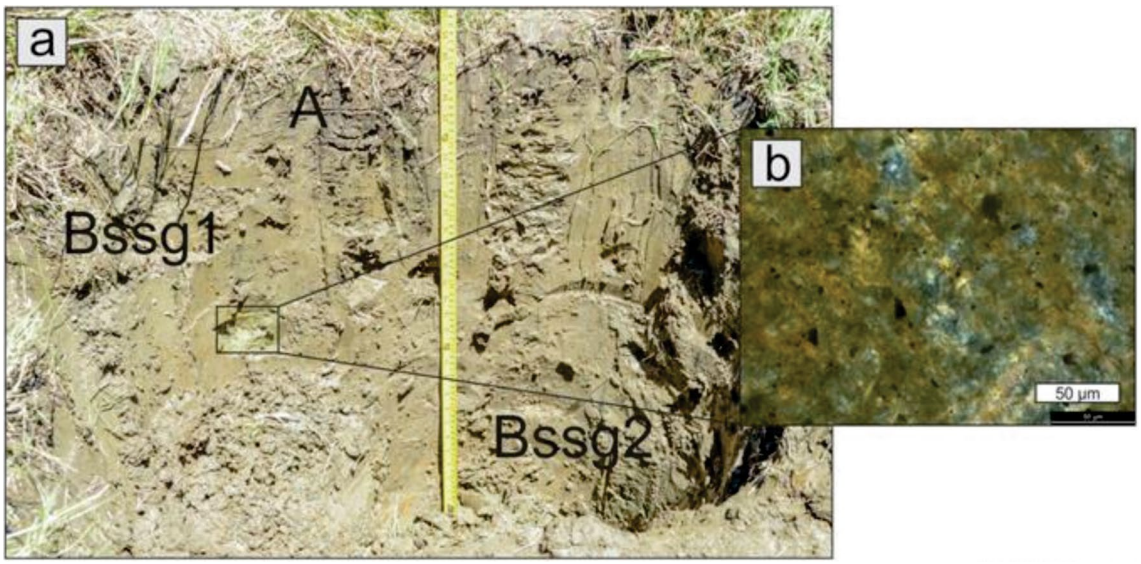

Fig. 2 **a** Field photo of a representative soil profile (E1) and **b** thin section of a Bssg horizon under parallel nicols, respectively. Note in (**b**) the gray—olive color typical of Fe-rich smectites

Bssg1 horizons). The descriptions and analysis performed by Imbellone and Mormeneo (2011) and other above-mentioned authors, allow us to classify these soils in WRB as Haplic vertisols (mollic, gleyic, grumic, humic, stagnic).

Smectites and illite are the dominant minerals (40–50 wt%), and kaolinite is about 10 wt% (Imbellone and Mormeneo 2011; Gómez Samus et al. 2017a; Montes et al. 2019). The parental material are clays mainly of detrital origin. They were deposited in an environment of very low energy, in brackish of shallow water. The sedimentation occurred at the same time as a flocculation processes in a saltmarsh under both fresh and saltwater conditions, during the late Holocene marine ingression (Cavallotto 1995; Gómez Samus et al. 2017a).

The origin of the clays is mainly related to the erosion of loessic soils, transported in suspension by streams that

flowed to the coastal plain and a tidal input of Río de la Plata, and probably with clay and silt particles derived from Paraná and Uruguay Rivers (Gómez Samus et al. 2017a). It is considered that pedogenesis started at the same time as clay deposition and continued once the saltmarsh was clogged and the retraction of the coastline reached the present position (Gómez Samus et al. 2017a, 2020). Even when the parental material cannot be recognized in situ, Imbellone and Mormeneo (2011) considered it was reddish. This is consistent with the reddish color (7.5YR) of the eroded loess successions (Imbellone and Teruggi 1993), and with the fact that the color of the water with suspended materials, not only in the Paraná and Uruguay Rivers but also in the Río de la Plata, is reddish to reddish brown (Depetris and Griffin 1968).

For the present work seven different hydromorphic vertisols profiles were analyzed (Fig. 1). From the gley horizons (Bssg) ten soil samples were collected at depths that vary from 20 to 110 cm; the coordinates are shown in Table 1.

Soil analyses

The description of the gley horizons was done at the field, it included the determination of wet color, texture and structure, as well as other relevant characteristics, such as vertic and redoximorphic features. Samples of approximately 1 kg were collected for laboratory tests. Besides, oriented samples in Kubiena boxes were obtained for thin sections.

The laboratory standard tests comprised the determination of dry color, grain size distribution, swelling test, organic matter content, pH and electric conductivity determinations. The color was determined by comparison with the Munsell color chart (Munsell 1912) for both, wet color at the field and dry color in the laboratory. Additionally, two representative (dry powder) samples were analyzed with a BYK Gardner Portable Spectrophotometer to obtain a strictly quantitative soil color record; the data was obtained in the CIELab system.

Grain size distribution was performed with wet sieving to estimate the amount of sand fraction, while silt and clay quantities were determined by the pipette analysis (Galenhause, 1971; Soil Survey Staff, 2014b). Hydrogen peroxide (H_2O_2; 30%) and hydrochloric acid (HCl; 1 M) were used to eliminate organic binders and carbonate cementation, while sodium hexametaphosphate [$(NaPO_3)_6$] dissolution at 5% was used as dispersive agent. Grain size intervals correspond to UddenWentworth scale and the swelling grade of clays by means of the so called Free-Swell-Test was applied in all the samples (Holtz and Gibbs 1956). The Walkley and Black (1934) humid combustion method was used (Van Reeuwijk 2002) for the determination of organic matter content. The

Table 1 Test pits location, color, grain size, swelling, organic matter, pH and electric conductivity of Bssg horizons samples

Site	Coordinates	Samples	Depth (cm)	Horizons	Munsell color (wet)	Grain size (%)			Free swelling (%)	Organic matter (%)	pH	Conductivity (dS/m)
						Sand	Silt	Clay				
1	34°51'35.0"S 57°59'12.7"O	PC1	23–51	Bssg1	5Y 4/2	0.5	26.9	72.7	320	0.39	8.1	2.46
		PC2	51–74	Bssg2	5Y 3/2	0.8	31.7	67.6	280	0.73	6.2	0.38
2	34°51'27.6"S 57°59'25.8"O	PC4	20–30	Bssg	5Y 3/2	0.8	11.1	88.1	250	0.55	7.9	1.79
3	34°51'53.4"S 57°59'21.4"O	PC5	40–68	Bssg	2.5Y 4/2	1.0	12.7	86.3	230	0.48	7.5	7.01
4	34°51'55.9"S 57°59'18.1"O	PC6	26–51	Bssg1	2.5Y 4.5/2	0.8	22.5	76.8	300	0.39	8.4	7.56
5	34°49'05.0"S 57°59'23.0"O	PC7	35–70	Bssg	5Y 5/1	1.0	28.6	70.4	230	0.51	6.5	1.1
		PC8	70–107	Bssg	5Y 4/1	2.6	28.7	68.8	180	0.38	7.9	4.29
6	34°49'05.0"S 57°59'48.5"O	PC9	36–60	Bssg	5Y 5/1	0.5	23.3	76.2	240	0.91	7.2	2.58
		PC10	60–105	Bssg	2.5Y 3/4	2.6	19.2	74.6	200	0.53	8.2	2.66
7	34°54'17.1"S 57°55'7.46"O	PC11	50–70	Bssg	5Y 5/2	2.0	26.8	71.2	246	0.68	8.1	3.07

pH and electrical conductivity were determined in saturated soil-paste extract, with 24 h rest.

Soils samples were examined by optical petrography and electron microscopy to determine the mineralogy of the different grains. Scanning electron microscopy (SEM) images were taken with a JEOL-JCM 6000 coupled with qualitative energy dispersive spectroscopy (EDS) and using standard sample preparation (thin gold coat). Other technical resources used consisted in applying X ray fluorescence (XRF), Mössbauer spectroscopy, measurement of magnetic parameters measurements, X-ray diffraction (XRD), including Greene-Kelly Test, and simultaneous differential thermal and thermogravimetric analysis (DTA–TG).

The chemical analysis of all samples was done with a spectrometer SPECTRO IQ. For every 5 g of sample it was added a binder (Binder BM-0002 Fluxana) with a ratio of 5:1, to avoid the movement of the grains during handling. Disk-shaped cubes were prepared with a diameter of 32 mm and 3—5 mm thick with a 15 tn press for the determination and quantification of Na, Mg, Al, Si, P, S, K, Ti, Mn and Fe, expressed as oxide.

Mössbauer spectra (± 12 mm/s) were obtained at room temperature in a conventional constant acceleration spectrometer in transmission geometry using a ^{57}CoRh source. Calibration was performed by an α-Fe foil (12 µm thick) and isomer shift was referred to this standard. The spectra fittings were carried out using a program that allows hyperfine magnetic fields and quadrupole splitting distributions. Samples were crushed and placed in plastic holders of 19 mm diameter and 300 mg to ensure the optimal signal/noise ratio (Long et al. 1983).

To determine the magnetic parameters, the dried and crushed samples were placed in plastic cubic boxes of 2 cm side and fixed with analytical sodium silicate. The magnetic susceptibility in low (χ_{lf}) and high frequency (χ_{hf}) was determined with a susceptibilimeter MS3 Bartington and a sensor MS2B. Then, the factor dependent on the frequency [$F\% = 100 \times (\chi_{lf} - \chi_{hf})/\chi_{lf}$] was calculated. pARM equipment attached to an alternating magnetic field demagnetizer (100 mT) and a minispin magnetometer (both Molspin Ltd.) were used to determine the anhysteretic remanent magnetization values ($ARM_{50\mu T}$ and $ARM_{90\mu T}$). The anhysteretic magnetic susceptibility (χ_{ARM}) was calculated. Curves of isothermal remanent magnetization (IRM) were achieved with a pulse magnetizer (ASC Scientific model IM-10–30), the Molspin Ltd minispin magnetometer was used. Once the maximum magnetization was reached ($IRM_{2,4\,T}$), applying reverse field, the coercivity remanence values (H_{cr}) and the coefficient $S_{\_ratio}$ ($IRM_{2,4\,T}/IRM_{\_300mT}$) were obtained. The concentration dependent parameters were standarized by the sample mass (χ_{lf}, χ_{ARM}, $IRM_{2,4T}$). Also, the magnetic susceptibility was determined with a MS2F sensor in samples heated at different temperatures and air cooled, the thermal process was done in an air-atmosphere for 2 h, at temperatures of 20, 100, 250, 350, 450, 550, 650, 750, 850, 950 and 1050 ºC.

Quantitative and qualitative XRD analysis of whole-rock powders and oriented preparations of the clay fraction were conducted using a Philips 3020 goniometer (Ni-filtered CuKa radiation, 40 kV, 20 mA, without secondary monochromator) and following the methodology described in Gomez Samus et al. (2017a and references therein).

The identification of clay minerals and the number of expandable layers within illite/smectite interstratified minerals were based on the position of characteristic reflexional lines (Moore and Reynolds 1997). The test of Greene-Kelly based on Li saturation, heating and glycerol solvation following sample preparation techniques described by Volzone (1991) was used to differentiate montmorillonite from other trioctahedral smectites such as iron-rich nontronite and beidellite.

The samples used for XRD were also used for the DTA-TG analysis; they were placed in PtRh crucibles in air atmosphere with a flow of 50 ml/min. Samples were calcinated up to 1050 °C at a heating rate of 10 °C/min using a Rigaku TG 8121.

Results

General characteristics of soil samples

Wet hue varies between 5Y and 2.5Y, while chroma is 2 (olive green) or less (Table 1) which is consistent with those values indicated by Imbellone et al. (2009) for soil samples taken at depths between 10 and 115 cm. The values obtained in the CIELab system were $L = 41.2$; $a = -0.7$; $b = 12.2$ (PC2) and $L = 51.1$; $a = -0.6$; $b = 7.6$ (PC8); the negative value of a component confirms that these are cold colors. These colors, together with the hydromorphic characteristics associated to endosaturation correspond to gleyic properties (IUSS Working Group WRB, 2014). In the air-dried samples the hue did not vary significantly, there was only an increase of the brightness value and slight chroma reduction. It should be noted that the color of the samples was homogenous; however, some yellowish mottles were observed. The thin section show a gray—olive color that was also observed in the hand-samples. In addition, it is also possible to recognize areas with Fe-oxides depletion pedofeatures and Fe-oxides quasi-coatings concentrations (Fig. 2b) (Stoops et al. 2010). SEM images have revealed aggregates of clay particles disposed in a face-to-face arrangement that indicate a detrital origin (Fig. 3a); however, the presence of very small crystals may suggest authigenic origin or partial transformation from clays or feldspar precursors (Fig. 3b). EDS analyses show Si, Al, Ca, Na, K, Mg in conjunction

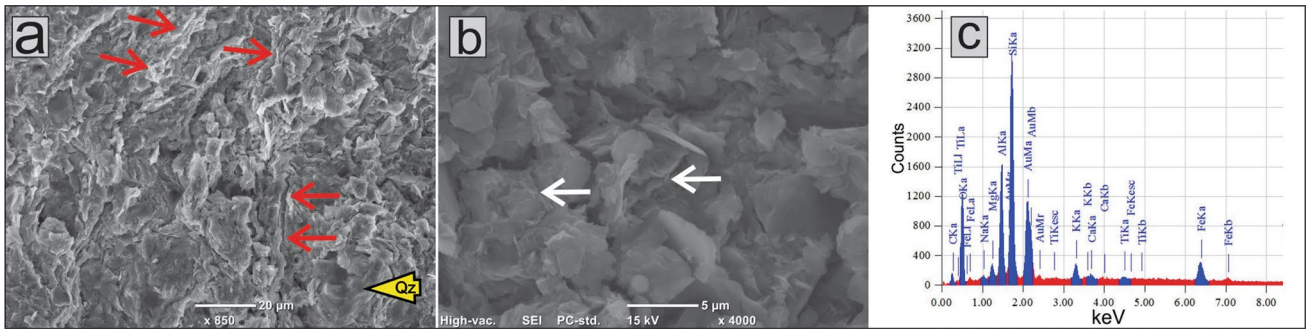

Fig. 3 SEM–EDS images of the clays. **a** Domains of face-to-face particle arrangement (red arrows) that form long aggregates. Silt-size quartz grains are floating in the clay-rich matrix. **b** Magnified view with randomly oriented clay particles. The presence of delicate clay crystals (white arrows) suggests an authigenic origin. **c** The EDS spectrum of clay particles

with high Fe that probably represent the composition of Fe-rich smectites (Fig. 3c).

The grain size distribution it is similar in all samples, with high amount of clay (> 65%) and little sand (< 2%) (Table 1); the textural type is clayey. The values obtained were like those obtained by Cappannini and Mauriño (1966), Giménez et al. (2005), Imbellone et al. (2009), Imbellone and Mormeneo (2011) and Montes et al. (2013).

The values of swelling are very high (180% to 320%), revealing an important presence of expandable minerals.

Organic matter is present in all the samples in low amounts (< 1%); which is consistent with results reported by other authors (Imbellone et al. 2009; and Montes et al. 2013).

Chemical composition and Mössbauer spectroscopy

Regarding the chemical composition, SiO_2 and Al_2O_3 are the prevailing elements and show great uniformity (Table 2). In order of abundance, the Fe_2O_3 content ranges between 9 and 12%, whereas Na_2O, K_2O and MgO show concentrations lower than 5%, with low variability. Whereas CaO shows concentrations between 0.7 and 5.2%, which may be related to local concentration of salt, such as bicarbonate or sulphate. There were also found TiO_2, SO_3, PO_2O_5 and MnO even though in lower amounts (< 1.5%), as also reported by Montes et al. (2019) for Mn oxide.

Mössbauer analysis revealed the presence of three iron environments, two corresponding to Fe^{3+} and one to Fe^{2+} (Fig. 4; Table 3), as well as a paramagnetic relaxation site (Murad 2010), which is associated with the existence of kaolinite. The amount of ferric iron in all the samples is more than 90% of the total iron content. Hyperfine parameters of the doublets show values concordant with the presence of smectite, illite and kaolinite. These results are consistent with those obtained by Montes et al. (2012) at depths between 30 and 50 cm. It is also in agreement with the Mössbauer data obtained in loess sequences of La Plata area (Bidegain et al. 2004), that focused in studying the variation of Fe^{2+} and Fe^{3+} in loess and paleosoils. The authors found that the Fe^{2+} concentration is four times lower in the paleosoils than in the loess layers.

Magnetic parameters

Values of the extensive magnetic parameters (χ_{lf}, χ_{ARM} and $IRM_{2,4\ T}$) are homogenous and relatively low, despite the high amount of iron (Table 4). Magnetic susceptibility (χ_{lf})

Table 2 Chemical elements expressed as oxides determined by X-ray fluorescence of the Bssg horizons samples

Sample	LOI550	Na_2O	MgO	Al_2O_3	SiO_2	PO_2O_5	SO_3	K_2O	CaO	TiO_2	MnO	Fe_2O_3
PC1	15.3	4.18	4.18	18.31	53.49	0.42	0.26	2.90	2.35	0.86	0.11	12.00
PC2	14.6	3.57	3.93	18.22	53.78	0.53	0.73	2.71	4.8	0.75	0.11	9.81
PC4	17.0	4.22	4.64	19.41	49.77	0.33	1.14	2.85	5.06	0.72	0.19	9.83
PC6	15.3	4.24	4.43	19.04	53.22	0.27	0.95	2.84	2.97	1.38	0.17	8.97
PC7	15.3	4.78	4.86	19.31	54.66	0.52	0.15	3.23	0.81	0.83	0.06	9.9
PC8	12.2	4.14	3.66	18.27	58.97	0.33	0.10	3.46	0.88	0.55	0.05	7.53
PC10	12.1	3.60	4.57	18.75	56.91	0.29	0.05	3.55	0.69	0.73	0.14	9.72
PC11	13.5	3.34	3.86	17.4	54.23	0.23	0.20	2.91	2.44	0.73	0.07	11.79
Average	*13.8*	*4.0*	*4.3*	*18.6*	*54.4*	*0.4*	*0.4*	*3.1*	*2.5*	*0.8*	*0.1*	*9.9*
	%	%	%	%	%	%	%	%	%	%	%	%

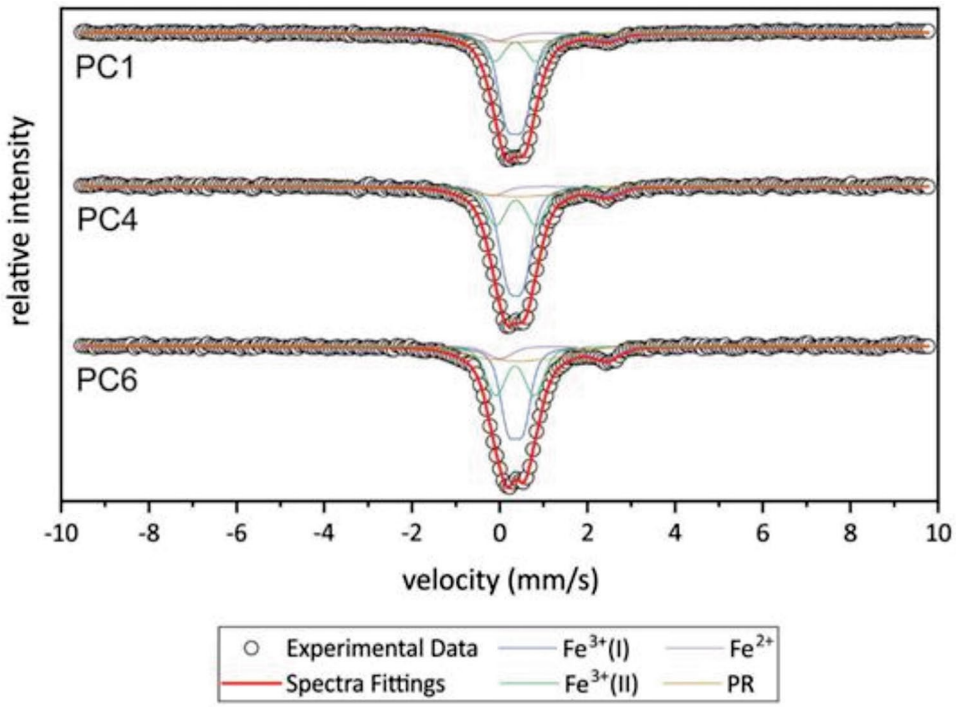

Fig. 4 Mössbauer spectra of PC1, PC4 and PC6. The open circles represent the experimental data. The solid red lines are the result of the fitting as described in the text

Table 3 Mössbauer hyperfine parameters obtained from Mössbauer spectra fittings

Sample	Fe^{3+} (I)			Fe^{3+} (II)			Fe^{2+}			Paramagnetic relaxation		
	δ	Δ	FR	δ	Δ	FR	δ	Δ	FR	δ	H	FR
PC1	0.35	0.37	51 ± 2	0.35	0.87	25 ± 2	1.22	2.47	7 ± 1	0.37	6.0	17 ± 2
PC4	0.36	0.36	51 ± 3	0.37	0.91	25 ± 3	1.14	2.63	7 ± 1	0.43	6.0	18 ± 2
PC6	0.36	0.36	47 ± 2	0.36	0.95	23 ± 2	1.19	2.58	9 ± 1	0.43	6.0	21 ± 2

δ, Δ and H are the isomer shifts referred to Fe (mm/s), the quadrupole splitting (mm/s), and the magnetic hyperfine field in T, respectively. Relative spectral area (%) of each Fe phase (FR) are also listed

Table 4 Magnetic parameters of the samples of Bssg horizons

Sample	χ_{if} (10^{-8} m^3/kg)	χ_{ARM} (10^{-8} m^3/kg)	$IRM_{2.4T}$ (10^{-3} Am^2/kg)	F% (%)	H_{cr} (mT)	S_{-300} (adim)	RRM (%)
PC1	14.8	25.2	0.63	1.1	81.8	0.57	33.4
PC2	12.8	24.3	0.61	1.7	91.3	0.55	34.5
PC4	12.0	24.8	0.45	2.1	103.4	0.49	37.3
PC5	13.6	26.0	0.58	1.8	77.7	0.54	32.1
PC6	12.3	23.0	0.61	0.0	97	0.51	36.1
PC7	11.9	25.1	0.45	1.1	89.9	0.59	31.6
PC8	13.2	43.2	1.13	3.3	72.8	0.75	20.9
PC9	12.4	20.3	0.44	2.0	100.8	0.49	36.4
PC10	16.6	36.3	1.05	0.7	68	0.59	28.9
PC11	18.7	34.0	0.95	3.6	83.1	0.57	32.3
PROM.	13.8	28.2	0.69	1.7	86.58	0.57	32.4

is lower than 20×10^{-8} m^3/kg, while anhysteretic magnetic susceptibility (χ_{ARM}) and maximum isothermal remanent magnetization ($IRM_{2,4\,T}$) are lower than 40×10^{-8} m^3/kg and 1.1×10^{-3} Am^2/kg, respectively, for all the samples. Correlation coefficient between χ_{ARM} and $IRM_{2.4\,T}$ is highly strong and positive ($R=0.95$), even though it is moderate between χ_{lf} and those parameters ($R=0.54$ and $R=0.67$, respectively). Correlation coefficient between total iron and χ_{lf} is moderate and positive ($R=0.5$), but null with χ_{ARM} and $IRM_{2.4\,T}$. Such behavior might be related to the contribution of paramagnetic minerals in the χ_{lf} values obtained, but those minerals do not participate in the X_{ARM} and $IRM_{2.4\,T}$ values. Regarding the susceptibility frequency dependent factor (F%), values lower than 4%, such as those recorded in this work would indicate a low contribution of superparamagnetic magnetite (Dearing et al. 1996).

Frequency-dependent magnetic susceptibility values and low susceptibility values of Pampean loess were compared with those ones of China and Siberia (Bidegain et al. 2005). The authors found that gleying during waterlog conditions have removed much of the magnetic material from certain stratigraphic intervals. Moreover, the depletion of the extensive magnetic values in hydromorphic layers has clearly been demonstrated in several loess profiles carried out in the Pampean region (Bidegain et al. 2009).

IRM Acquisition curves (Fig. 5a) indicate saturation in magnetic fields higher than 1000 mT, which is a typical behavior of high coercivity substances such as

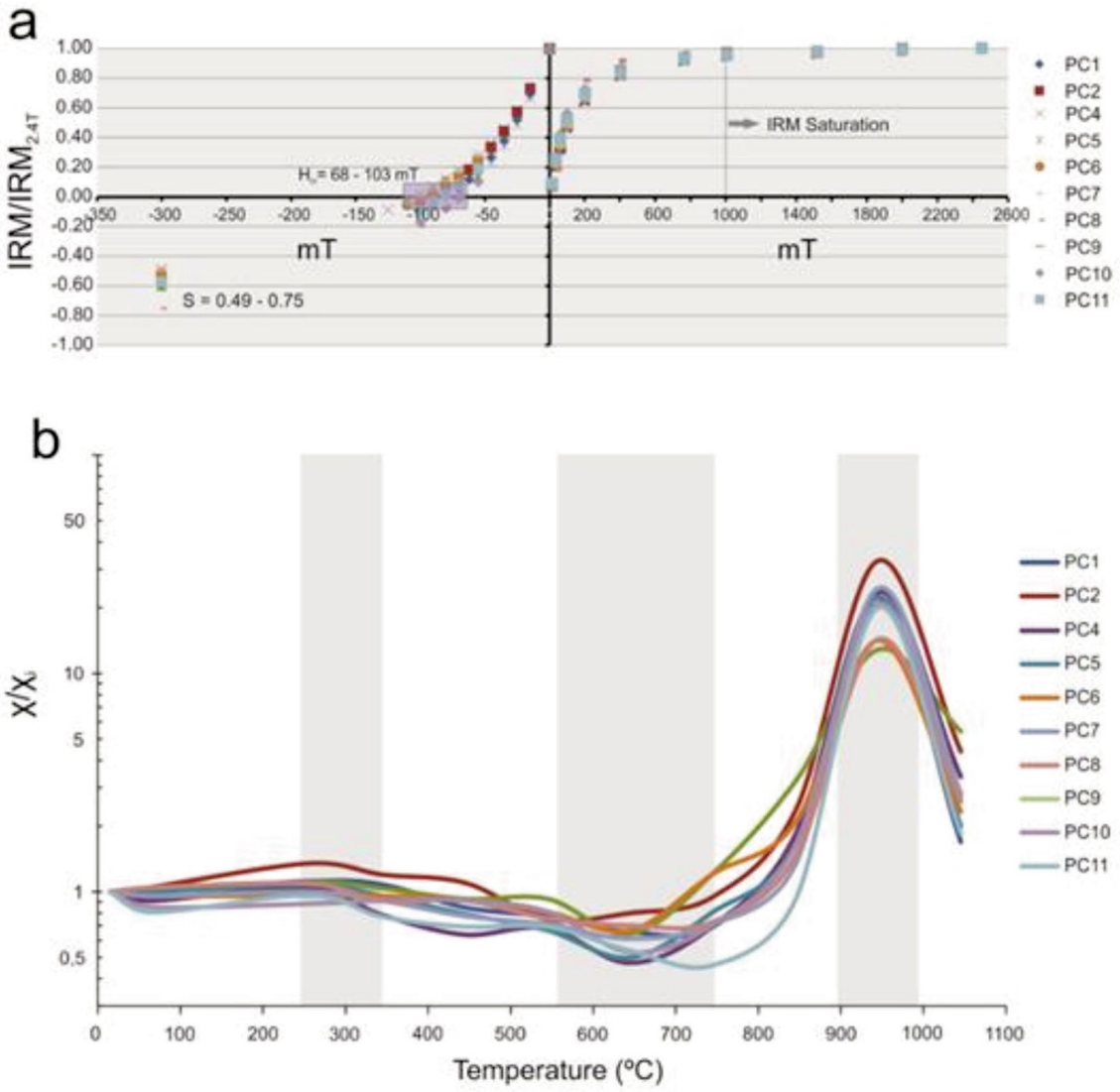

Fig. 5 **a** Acquisition of isothermal remanent magnetization curves and back field of samples from the Bssg horizons. Note that saturation begins at 1000 mT, which is a typical behavior of antiferromagnetic substances. **b** Standardized magnetic susceptibility curves as a function of calcination temperature until 1050 ºC. Note the appearance and disappearance of magnetic phases at 250–350, 550–750 and 900–1000 ºC (see the explanation in the text)

hematite—goethite (Thompson and Oldfield 1986). Remanence coercivity (H_{cr}), S coefficient and residual remanent magnetization (RRM) (Table 4) indicate an important participation of high coercivity species as goethite.

Bartel et. al. (2005) applying magnetic parameters in the study of argiudoll and epiaqualf soils of La Plata area, indicate that the intrazonal soils such as the mentioned epiaqualf, developed under conditions of high humidity. They showed the same general susceptibility pattern than the argiudoll soil but with much lower values. Furthermore, they consider that this is a recent phenomenon—in geological terms—of alteration (dissolution in aqueous environment) of ferrimagnetic minerals (magnetite) and neoformation of more oxidized compounds (Fe_2O_3 and FeOOH) of the type hematite, goethite.

Magnetic susceptibility curves in function of temperature (Fig. 5b) showed mineralogic transformations that involve the development and destruction of magnetic phases. The gradual increase between 250 and 350 °C may be in concordance with the dihydroxylation of iron oxy-hydroxides, such as goethite and ferrihydrite and the resulting maghemite formation (Eggleton and Fitzpatrick 1988; Ketterings et al. 2000; Barrón and Torrent 2002). For temperatures higher than 350 °C, susceptibility decreases gradually until they reach the lowest at temperatures between 550 and 750 °C, which may correspond to hematite complete transformation (Gómez Samus et al. 2017a, c). Susceptibility increases together with temperature until it reaches the maximum at 950 °C which could be related to Ca presence (Gómez Samus et al. 2017b, c), and finally decreases..

X- ray diffraction

Diffraction patterns indicate a predominance of clay minerals (around 60%), while secondary mineral phases include quartz, plagioclase and alkaline feldspar with minor proportions of calcite and probably iron oxide hydroxide such as goethite and ferrihydrite (Fig. 6, Table 5). Whole-rock diffractograms show a hump between 24º and 32º 2θ related to mineral phases of low crystallinity or associated to amorphic substances (Grathoff and Moore 1996). This feature is not related to a high content of iron oxy-hydroxide, since there is

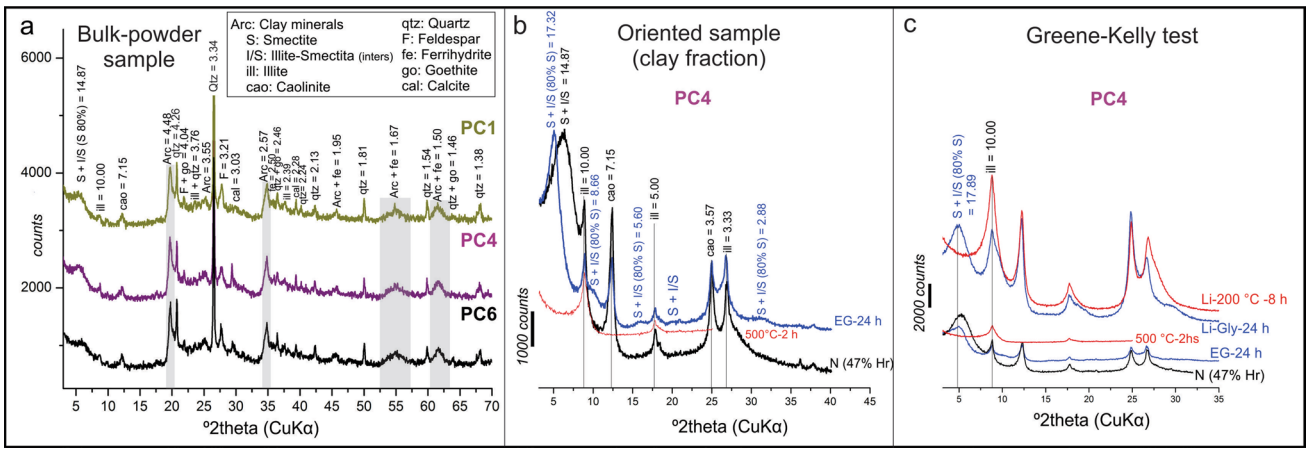

Fig. 6 X-ray diffractograms of bulk-powder of Bssg representative samples (**a**) and oriented sample (**b**) with N: natural; G: glycol-24hs and C: calcined-550 ºC oriented preparations. Values are expressed in Å. **c** Results of the Greeny Kelly test. Note the expansion of the Sm peak after the Li-200 °C and glycerol (Gly) solvation

Table 5 Quantitative XRD analysis (bulk-rock samples) of the Bssg horizons obtained by Rietveld method

Sample	Minerals						
	Smectite (+I/S)	Illite	Caolinite	Quartz	Feldspars	Calcite	Iron Oxy-hydroxides (goethite)
PC1	28.08 (1.14)	20.40 (0.97)	10.06 (0.87)	23.32 (1.01)	16.31 (0.87)	< 2	< 2
PC4	35.98 (2.05)	19.84 (1.05)	10.67 (1.23)	19.61 (1.29)	11.49 (1.17)	2.10 (1.41)	< 2
PC6	32.69 (2.79)	23.95 (1.15)	10.71 (0.83)	18.23 (1.31)	12.97 (1.05)	< 2	< 2

The values are expressed in wt% with their standard errors. Feldspars include plagioclase and alkaline feldspar, whereas Iron Oxy-hydroxides are goethite and ferrihydrite

no fluorescence associated to a background increase (Moore and Reynolds 1997). The diffraction peaks corresponding to 4.48 Å, 2.57 Å and 1.50 Å are relatively wide, which indicate low crystallinity or a high disorder degree indicating the predominance of smectite. The diffraction peak of the plane 060 between 61.67º 2θ and 62.22º 2θ positioned close to 1.49 Å (Fig. 6a) and indicates the predominance of dioctahedral clay minerals (Fig. 6a) equivalent to minerals of the montmorillonite–beidellite series (Moore and Reynolds 1997).

On the oriented natural samples patterns, the typical reflections at 15 Å, 10.00 Å, 5.00 Å and 3.33 Å indicate the presence of smectite besides of illite. Two other diffraction lines of important intensity correspond to 7.15 Å and 3.57 Å which denote the presence of kaolinite. The ethylene–glycol salvation patterns show the displacement to 17.3 Å typical in smectites (Fig. 6b). However, diffraction lines at 8.66 Å and 5.60 Å and around 3.33 Å, suggest the existence of illite/smectite (I/S) interstratified minerals, consistent with Montes (2013), with high amount (80%) of expansive layers. The non-swelling behavior and the collapse of the structure after heating confirm the presence of kaolinite, while the collapse of smectite-I/S shift to 9.99 Å at the position of illite. The samples treated with Li-200 ºC-glycerol solvation do not show the irreversible collapse of the structure due to Li-ions moving into the vacant octahedral sites (Volzone 1991). The expansion of the structure giving a broad XRD reflection at 17.9 Å indicates the identification of beidellite-nontronite clay minerals (Fig. 6c).

DTA-TG

DTA and TG curves, such as those shown in Fig. 7, indicate a first endothermic peak around 75 °C, with a mass loss of 5–7%, from the beginning of the thermal process until a temperature of around 150 ºC. This process is attributed to adsorption water loss (hygroscopic) mainly from clay minerals. There is a second endothermal peak around 260–280 ºC along with a slight mass loss (< 3%), associated to the dehydroxylation of iron oxy-hydroxides, such as goethite (Romero Gómez et al. 2013). This suggests that an important part of the high coercivity signal observed in the magnetic characteristics correspond to hydrated species, particularly goethite. Between 400 and 410 ºC, a slight inflexion in the DTA curve is observed, which may correspond to an exothermal peak of organic material combustion, which, as previously mentioned, was found in relatively low amounts (less than 1%). The second important endothermal peak was registered between 480 and 495 ºC, along with a mass loss of 5–8%, due to dehydroxylation of clay minerals (Grim and Rowland 1942; Frost et al. 2000). Finally, between 800 and 900 ºC there is an inflexion of DTA curve, which might be related to endothermic peaks, associated with calcite decarbonization, or exothermal peaks related to crystallization of new anhydrous phases.

These results are consistent with the Fe-smectite presence. Taking into account that in Al-rich montmorillonite dehydroxylation occurs around 600–700 ºC, the incorporation of Fe^{3+} in the crystalline structure (replacing Al^{3+}

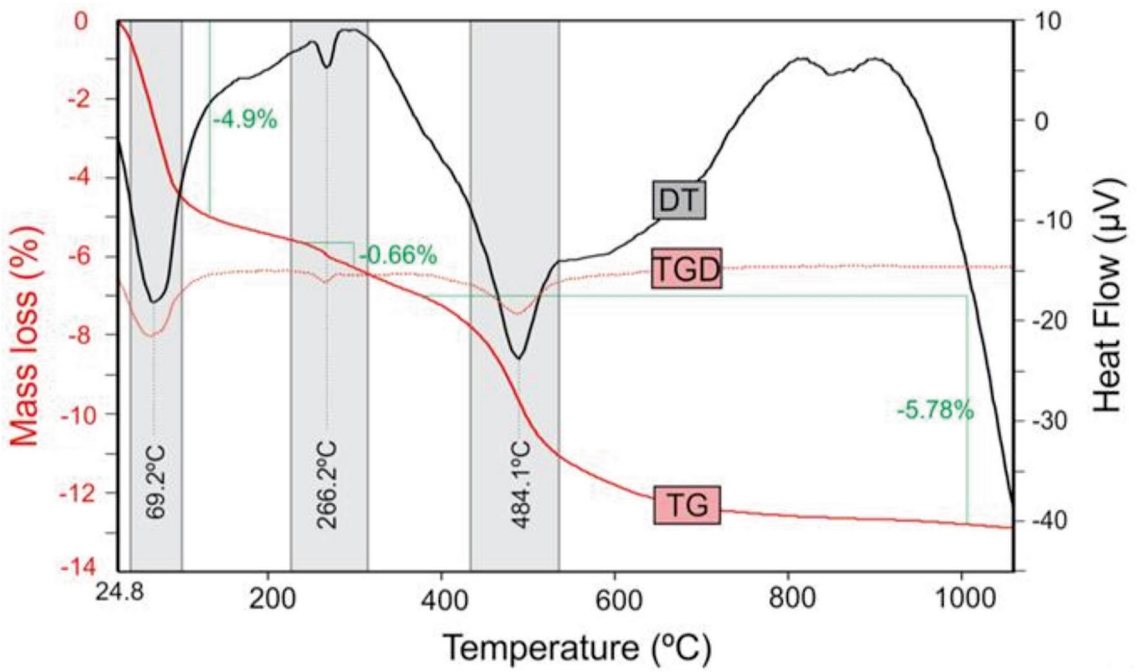

Fig. 7 Differential thermal (DT) and thermogravimetric (TG) analyses curves of PC6 sample

in the octahedral layer), induces an important decreases to 400–500 ºC for Fe-smectite (Grim and Rowland 1942; Frost et al. 2000) as documented in the present work.

Discussion

Minerals with iron in gley horizons

The data analysis allows us to infer that goethite is the prevailing iron oxide in the soil samples from the coastal plain of the Río de la Plata estuary. The pH conditions close to neutral and Eh values around 0 V (Imbellone et al. 2009) are consistent with the preservation, and even with the authigenesis of goethite (Fig. 8). However, it is not dismissed the possibility of other oxy-hydroxide participation, such as ferrihydrite. Mössbauer spectra do not show magnetic signal corresponding to goethite (sextets); therefore, goethite particles should be smaller than 15 nm (Vandenberghe 1991).

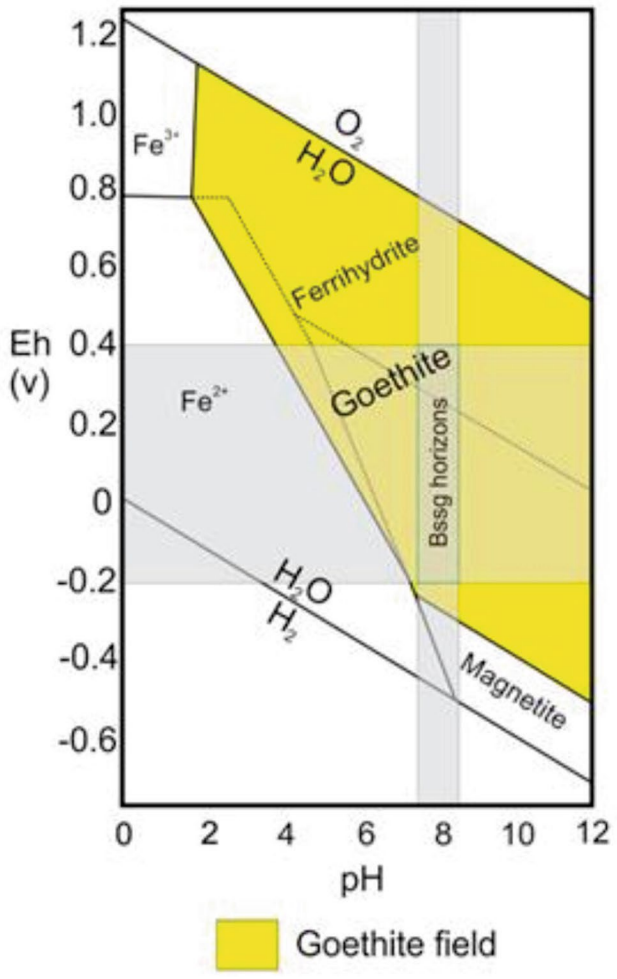

Fig. 8 pH vs. Eh graph after Skinner and Fitzpatric (1992). Note that these parameters values for the Bssg horizons are plotted in the goethite and ferrihydrite fields

The low amount of oxy-hydroxide (< 3%) is not enough to explain the high total iron concentration in the studied samples. As previously mentioned, ferric iron is the dominant Fe specie and it would be related mainly to minerals with paramagnetic behavior. In this context, it is worth to consider the composition of clay minerals, mainly smectites followed by illite that based on the Greene-Kelly test indicated the presence of iron-rich smectites (Fe-beidellite/nontronite); also corroborated by the endothermic peak in the DTA curve and magnetic values.

The iron incorporation on clay structures would be an authigenic process, as mentioned for saltmarsh environments (de Souza- Júnior et al. 2010), where cyclic changes in the redox potential promote pyrite oxidation and the subsequent nontronite neoformation, in presence of Si, Mg and Al (Fernandez-Caliani et al. 2004). Although pyrite was not detected, it is probable that it might had been present during the Holocene saltmarsh that gave origin to the parental material of these soils (Cavallotto 1995; Gómez Samus et al. 2017a, 2020). Furthermore, it cannot be dismissed that iron-rich smectite could be a consequence of illite transformation, a process that occur in high salinity conditions and redox variation in presence of iron (Komadel et al. 1995; Velde and Church 1999). Therefore, it is considered that iron-rich smectites are the result of a combination of particular settings in an environment with repeated wet—dry cycles, where Eh variations in a slightly alkaline conditions would have favored the incorporation of iron in the structure of smectites.

Considering Mössbauer spectra and previous analyzes (Montes et al. 2016), illite would be the main Fe^{2+} carrier. However, there is a possibility that ferrous iron is found, in small proportions, in minerals that could not be identified by these means. For example, framboidal pyrite, was described in saltmarsh environments, like the one that gave origin to the parental materials of the analyzed soils (Ferreira et al. 2007; Otero et al. 2009; Rios et al. 2018). Given the presence of sulphur in chemical analysis, it is possible to consider that pyrite constituted a mineral phase in the sediments, which due to the change in pedogenic conditions after the saltmarsh desiccation, may have oxidized and a part of the iron included in smectites and sulfates (Zhang and Evangelou 1996). Based on phosphorous existence, it is possible to consider the presence of ferrous iron phosphate such as vivianite, usually found in anoxic soils and sediments (Roden and Edmonds 1997). Finally, it is worth mentioning that the existence of green rusts was dismissed due to the permanence of the hue once the sample was dried. Its greenish blue component is easily oxidized when exposed and turn reddish (Scheinost 2005).

Ferric iron and gley colors in Pampean sediments

It is possible to consider two minerals as stains with ferric iron that generate gley colors in hydromorphic vertisols of Río de la Plata coastal plain. On the one hand, iron-rich smectites are green, olive green, greenish yellow to yellow (Stucki 1988), such as the Fe-beidellite from weathered volcanic rocks in *Patagonia* shown in Fig. 9a (Cravero et al. 2014). On the other hand, goethite is usually yellow (Schwertmann and Fitzpatrick 1992; Scheinost 2005) and is artificially created in paint industry (ferrite yellow) (Lozano 1978). To illustrate it, acrylic paints were used to reproduce the color pattern (Fig. 9b). This may be the way in which goethite together with organic material or low luminosity minerals, would contribute to greenish colors of the soils.

Based on these considerations, the ferrous iron influence in gley colors of hydromorphic vertisols of Río de la Plata coastal plain was rejected. Goethite effect on gley colors is like that observed by Vodyanitskii et al. (2005, 2007), but also, in these soils it is highlighted the influence of ferric iron-rich smectites.

An important aspect to be pointed out refers to the participation of ferric iron in gley horizons of loessic successions of Pampean loess (Bidegain et al. 1995, 1996), such as shown in Fig. 10. The presence of hydromorphic paleosols is common in these sequences which colors differ from the typically reddish pampean loess (7.5YR) to greener hue (5Y) (Imbellone and Teruggi 1993; Gómez Samus 2016). Studies carried out in sequences of loess/paleosols of La Plata area, allowed to determine that gley horizons presented lower Fe^{2+} concentration (0.02%) than the less pedogenized loess

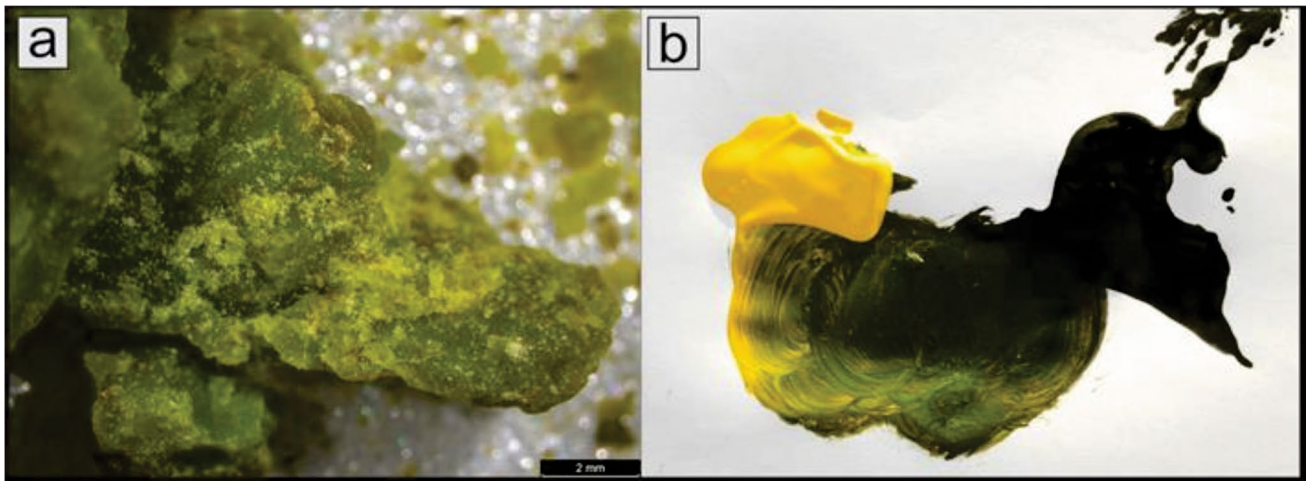

Fig. 9 Photographs showing the color on Bssg horizons. **a** Fe-rich beidellite under the loupe (Sample courtesy of Fernanda Cravero). **b** Gley colored pattern reproduced by acrylic paints, note that the darkening of the yellow paint is seen as green

Fig. 10 Typical Pampean loess profile on the Atlantic coast of Mar del Plata. Note the contrast between gley and reddish horizons

layers (0.40%) (Bidegain et al. 1995, 1996). Moreover, in those levels, where the content of titanomagnetites and ferrous iron increase, the highest susceptibility values (loess layers) were obtained. Conversely, the gley horizons, with lowest Fe^{2+} content, show the lowest susceptibility values (Bidegain and Rico 2004; Bidegain et al. 2005, 2009).

Conclusions

The current results allow us to reconsider some assumptions about the pigments that give rise to olive colors in soils with gleyic and stagnic properties. The main statements that stand out here are: (1) Ferric iron (Fe^{3+}) bearing minerals give the olive colors (gley) in the hydromorphic vertisols of the coastal plain of the Río de la Plata. (2) The minerals with ferric iron are Fe-rich smectites (Fe-Beidellite/Nontronite) of green, olive green, greenish yellow to yellow colors, as well as goethite, usually yellow. (3) This pattern can be related to other olive-colored hydromorphic soils, for instance in the loessic soils and paleosoils of the Pampean region.

Acknowledgements We would like to gratefully acknowledge the financial support from PICT-2016-0146 encouraging the development of the Project "Environmental Magnetism and Paleomagnetism in soils of La Plata and surrounding areas". Thanks to the researchers and institutions for giving their support; the Technological Center for Mineral and Ceramic Resources (CETMIC-CONICET-CIC-UNLP), the Institute of Physics "Arroyo Seco" (IFAS-CIFICEN-CONICET) of Tandil, the Institute of Physics (Facultad de Ciencias Exactas—UNLP), the Institute of Geomorphology and Soils (IGS-UNLP) and the Laboratory for Technological Research (LEMIT-CIC). Special thanks to the professors Mario Da Silva and Martín Hurtado of General Pedology at FCNyM in the University of La Plata, for their collaboration and advice during the field work. And last but not least, we would like to thank Dra. Fernanda Cravero for providing a Fe-Beidellita sample that is included in the present investigation. This article was funded by MinCyT (PICT-2016-0146) (Grant no. 2500).

References

Barrón V, Torrent J (2002) Evidence for a simple pathway to maghemite in Earth and Mars soils. Geochim Cosmochim Acta 66:2801–2806

Bartel A, Bidegain JC, Sinito A (2005) Propiedades magnéticas de diferentes suelos del Partido de La Plata, provincia de Buenos Aires. Revista de la Asociación Geológica Argentina 60:591–598

Bidegain JC, Rico Y (2004) Mineralogía magnética y registros de susceptibilidad en sedimentos cuaternarios de polaridad normal (Brunhes) y reversa (Matuyama) de la cantera de Juárez, provincia de Buenos Aires. Revista de la Asociación Geológica Argentina 59:451–461

Bidegain JC, Iasi RR, Pérez RH, Pavlicevic R (1995) Correlación de Parámetros Magnéticos con la Concentración de Óxido Ferroso en Sedimentos Cuaternarios de la Localidad de Hernández, La Plata. Provincia de Buenos Aires. IV Jornadas Geológicas y Geofísicas Bonaerenes Acta I:177185, Junín.

Bidegain JC, Pavlicevic R, Iasi R, Pérez R (1996) Susceptibilidad Magnética y Concentraciones de FeO en Loess y Paleosuelos Cuaternarios como Indicadores de Cambios Paleoambientales y Paleoclimáticos. XIII Congreso Geológico Argentino y III Congreso de Exploración de Hidrocarburos Actas II:521535, Buenos Aires.

Bidegain JC, Terminiello L, Rico Y, Mercader RC, Aragón E (2004) Mineralogía Magnética en la Transición Brunhes/Matuyama. Pleistoceno de la Provincia de Buenos Aires. Argentina. Revista de la Asociación Geológica Argentina 59:193–199

Bidegain JC, Evans ME, van Velzen AJ (2005) A magnetoclimatological investigation of Pampean Loess, Argentina. Geophys J Int 160:55–62

Bidegain JC, Rico Y, Bartel A, Chaparro M, Jurado S (2009) Magnetic parameters reflecting pedogenesis in Pleistocene Loess Deposits of Argentina. Quatern Int 209:175–186

Cappannini, D, Mauriño V (1966) Suelos de la zona litoral estuárica comprendida entre las ciudades de Buenos Aires al norte y La Plata al sur. INTA. Colección Suelos, 45 pp, Buenos Aires.

Cavallotto JL (1995) Evolución geomorfológica de la llanura costera ubicada en el margen sus del Río de la Plata. Tesis Doctoral 635. Facultad de Ciencias Naturales y Museo, Universidad Nacional de La Plata, 237 pp

Cornell RM, Schwertmann U (1996) The iron oxides: Structure, properties, reactions, occurrence and uses, 1st edn. Wiley, Weinheim, p 703

Cornell RM, Schwertmann U (2003) The iron oxides: structure, properties, reactions, occurrence and uses, 2nd edn. Wiley, Weinheim, p 664

Cravero F, Marfil SA, Ramos CP, Maiza P (2014) Coexistence of halloysite and iron bearing clays in an altered ignimbrite, Patagonia, Argentina. Clay Miner 49:429–441

Daniels RB, Simonson GH, Handy RL (1961) Ferrous iron content and color of sediments. Soil Sci 91:378–382

de SouzaJúnior VS, VidalTorrado P, GarcíaGonzález MT, Macías F, Otero XL (2010). Smectite in mangrove soils of the State of São Paulo, Brazil. Scientia Agricola 67:4752

Dearing JA, Dann RJL, Hay K, Lees JA, Loveland PJ, band O'Grady K (1996) Frequency-dependent susceptibility measurements of environmental materials. Geophysical Journal International 124:228–240

Depetris PJ, Griffin JJ (1968) Suspended Load in the Río de la Plata drainage basin. Sedimentology 11:53–60

Eggleton RA, Fitzpatrick RW (1988) New data and a revised structural model for ferrihydrite. Clays Clay Miner 36:111–124

FernandezCaliani JC, Crespo E, Rodas M, Barrenechea JF, Luque FJ (2004) Formation of nontronite from oxidative dissolution of pyrite disseminated in precambrian felsic metavolcanics of the southern Iberian massif (Spain). Clays and Clay Minerals 52:106114

Ferreira TO, VidalTorrado P, Otero XL, Macías F (2007) Are mangrove forest substrates sediments or soils? A case study in southeastern Brazil. Catena 70:7991

Frost RL, Ruana H, Kloprogge JT, Gates WP (2000) Dehydration and dehydroxylation of nontronites and ferruginous smectite. Thermochim Acta 346:63–72

Galenhouse J (1971) Sedimentation analysis. Carver R (ed) Procedures in sedimentary petrology. WileyInterscience, New York, 6594

Gaucher G (1971) Tratado de Pedología Agrícola. El suelo y sus características agronómicas. Ediciones Ómega, Barcelona, p 647

Giménez JE, Cabral M, Hurtado MA, Martínez OR, Sanchez CA, Da Silva MM, Forte L, Crincoli AC, Muntz D (2005) Elaboración y Transferencia de Cartografía Temática e Implementación de un Sistema de Información Geográfica para el Planeamiento (Partido de Berisso). Comisión de Investigaciones Científicas, Provincia de Buenos Aires, 70 pp

Gómez Samus ML (2016) Magnetoestratigráfia y parámetros magnéticos en sedimentos del Cenozoico tardío del sector Tandil-Balcarce-Mar del Plata: La Plata, Argentina, Universidad Nacional de La Plata, Tesis Doctoral, 430p. http://sedici.unlp.edu.ar/handle/10915/52323

Gómez Samus ML, Comerio M, Boff LD, Montes ML, Ontivero PE, Mercader RC, Bidegain JC (2017a) Minerales con hierro en arcillas vinculadas a la ingresión marina holocena en la llanura costera del estuario del Río de la Plata (Argentina): Implicancias paleoambientales. Latin Am J Sedimentol Basin Anal 24:61–83

Gómez Samus ML, Rico Y, Ziccarelli S, Parodi AV, Bidegain JC (2017b) Efectos del contenido de $CaCO_3$ inicial en las propiedades magnéticas de sedimentos calcinados. Resultados preliminares. Boletín de la Sociedad Geológica Mexicana 69:261–278

Gómez Samus ML, Rico Y, Gusso M, Canosa M, Bidegain JC (2017c) La susceptibilidad magnética como indicadora de temperaturas de calcinación de suelos. Relación con el contenido de calcio. Ciencia y Tecnol de los Materiales 7:7–16

Gómez Samus ML, Olivo M, Rico Y, Cellone F, Bidegain JC (2020) Magnetismo ambiental y sedimentología en una sucesión del Pleistoceno temprano—Antropoceno, en la costa sur del Río de la Plata: implicancias estratigráficas y paleoambientales. Revista de la Asociacion Geológica Argentina 77:144–162

Grathoff GH, Moore DM (1996) Illite polytype quantification using wildfire calculated Xray diffraction patterns. Clays Clay Miner 44:835–842

Grim RE, Rowland RA (1942) Differential thermal analysis of clay minerals and other hydrous materials. Part 1. Am Mineralogist 27:746–761

Holtz WG, Gibbs HJ (1956) Engineering properties of expansive clays. Transactions ASCE 121:641–677

Imbellone PA, Mormeneo L (2011) Vertisoles hidromórficos de la planicie costera del Río de la Plata, Argentina. Ciencias del Suelo 29:107–127

Imbellone PA, Teruggi ME (1993) Paleosols in loess deposits of the Argentine Pampas. Quaternary Int 17:49–55

Imbellone PA, Guichon BA, Giménez JE (2009) Hydromorphic soils of the Río de la Plata Coastal Plain, Argentina. Latin Am J Sedimentol Basin Anal 16:3–18

Imbellone PA, Gimenez JE, Panigatti JL (2010) Suelos de la región pampeana: Procesos de formación. Ed INTA, Buenos Aires. 320 pp

IUSS Working Group WRB (2006) World reference base for soil resources 2006. World Soil Resources Reports No. 103. FAO, Rome

IUSS Working Group WRB (2014) World Reference Base for Soil Resources 2014, update 2015 International soil classification system for naming soils and creating legends for soil maps. World Soil Resources Reports No. 106. FAO, Rome

Ketterings QM, Bigham JM, Leperche V (2000) Changes in soil mineralogy and texture cause by SlashandBurn Fires in Sumatra, Indonesia. Soil Sci Soc Am J 64:1108–1117

Komadel P, Madejova J, Stucki J (1995) Reduction and reoxidation of nontronite: questions of reversibility. Clays Clay Miner 43:105–110

Long GJ, Cranshaw TE, Longworth G (1983) The ideal Mössbauer effect adsorbent thicknesses. Mössbauer Effect Reference Data J 6:42–49

Lozano RD (1978) El color y su medición. Américalee S.R.L. Ed. Buenos Aires, 640 pp

Montes ML (2013) Estudio radiológico gamma de suelos de la zona aledaña a la ciudad de La Plata, provincia de Buenos Aires: modelado de perfiles de actividad y correlaciones con las propiedades del suelo. Tesis Doctoral. Facultad de Ciencias Exactas, Universidad Nacional de La Plata, 190 pp. http://sedici.unlp.edu.ar/bitstream/handle/10915/27104/Documento_completo.pdf?sequence=1&isAllowed=y

Montes ML, Mercader RC, Taylor MA, Runco J, Desimoni J (2012) Assessment of natural radioactivity levels and their relationship with soil characteristics in undisturbed soils of the northeast of Buenos Aires province. Argentina J Environ Radioactivity 105:30–39

Montes ML, Silva LMS, Sá CSA, Runco J, Taylor MA, Desimoni J (2013) Inventories and concentration profiles of ^{137}Cs in undisturbed soils in the northeast of Buenos Aires Province, Argentina. J Environ Radioact 116:133–140

Montes ML, Rivas PC, Taylor MA, Mercader RC (2016) Approximate total Fe content determined by Mössbauer spectrometry: application to determine the correlation between gammaray emmiter activities and total Fe content of Fe phases in soils of the Province of Buenos Aires. Argentina J Environ Radioactivity 162–163:113–117

Montes ML, Fernandéz MA, Brendlé J, Michelin L, Taylor MA, Torres Sánchez RM (2019) Co^{2+} sorption capacity indicators of La Plata region´s soils. Insights and correlations with soil properties. Int J Environ Health 9:3:224

Moore DM, Reynolds RCJ (1997) X-ray diffraction and the identification and analysis of clay minerals. Oxford, New York

Munsell AH (1912) A pigment color system and notation. Am J Psychol 23:236–244

Murad E (2010) Mössbauer spectroscopy of clays, soils and their mineral constituents. Clay Miner 45:413–430

Nickerson D, Kelly KL, Stultz KF (1945) Color of soil. J Opt Soc Am 35:297–300

Otero XL, Ferreira TO, HuertaDíaz M, Partiti CSM, Souza JrV, Vidal-Torrado P, Macías F (2009) Geochemistry of iron and manganese in soils and sediments of a mangrove system, Island of Pai Matos (Cananeia SP, Brazil). Geoderma 148:318335

Retallack GJ (2001) Soils of the Past. An introduction to Paleopedology 2nd Ed. Blackwell Sience Ltd, Eugene

Rios I, Bouza PJ, Bortolus A, Alvarez MP (2018) Soil-geomorphology relationships and landscape evolution in southwestern Atlantic tidal salt marsh in Patagonia, Argentina. J S Am Earth Sci 84:385–398

Roden EE, Edmonds JW (1997) Phosphate mobilization in iron rich anaerobic sediments: Microbial Fe (III) oxide reduction versus ironsulfide formation. Archiv für Hydrobiol 139:347–378

RomeroGómez P, González JC, Bustamante A, RuizConde A, Sánchez-Soto PJ (2013) Estudio in-situ de la transformación térmica de limonita utilizada como pigmento procedente de Perú. Boletín de la Sociedad Española de Cerámica y Vidrio 52:127131

Scheinost AC (2005). Metal Oxides. In Hillel D (ed) Encyclopedia of Soils in the Environment Elsevier, Oxford, 428–438

Schulze FG, Nagel GE, Van Scoyoc GE, Henderson TL, Baungardner MF, Stott DE (1993). In: Soil Color. SSSA Special Publication no. 31. Soil Science Society of America, 71–90

Schwertmann U, Fitzpatrick RW (1992) Iron minerals in surface environments. In: Skinner HCW and Fitzpatrick RW (eds) Biomineralization, Processes of Iron and Manganese. Catena Supplemet 730

Soil Survey Staff (2014a) Keys to soil taxonomy, 12th edition. USDA Natural Resources Conservation Service.

Soil Survey Staff (2014b) Kellogg Soil Survey Laboratory methods manual. Soil Survey Investigations Report No. 42, version 5.0.

Stoops G, Marcelino V, Mees F (2010) Interpretation of micromorphological features of soils and regoliths. Elsevier, Amnsterdam, Oxford

Stucki JW (1988) Structural Iron in Smectites. In: Stucki JW, Goodman BA, Schwertmann U (eds) Iron in soils and clay minerals, D. Reidel, Dordrecht, pp 625–675

Thompson R, Oldfield F (1986) Environmental magnetism. Allen and Unwin, London

Thorp J, Smith GD (1949) Higher categories of soil classification: order, suborder, and great soil groups. Soil Cuence 67:117–126
Van Reeuwijk LP (2002) Procedures for soil analysis. Wageningen, International Soil Reference and Information Centre. Wageningen, p 119
Vandenberghe RE (1991) Mössbauer spectroscopy and applications in geology. International Training Centre for PostGraduate Soil Scientistis, 2nd ed, State University Gent, 88 pp.
Velde B, Church T (1999) Rapid clay transformation in Delaware salt marshes. Appl Geochem 14:559–568
Vepraskas MJ, Wilding LP (1983a) Albic Neoskeletans in Argillic Horizons as Indices of Seasonal Saturation and Iron Rduction. Soil Sci Soc Am J 47:1202–1208
Vepraskas MJ, Wilding LP (1983b) Aquic moisture regimes in soils with and without low chroma colors. Soil Sci Soc Am J 47:280–285
Vodyanitskii YN, Vasil´ev AA, Gilev VY (2007) Iron minerals in soils on red-earth deposits in the Cis-Ural Region. Eurasian Soil Sci, 40:432–444
Vodyanitskii YN, Shishov LL, Vasil´ev AA, Sataev EF (2005) An Analysis of the color of forest soils on the Russian plain. Eurasian Soil Science, 38:11–22
Volzone C (1991) Improvements in the method to differentiate montmorillonite from other smectites. J Materials Sci Lett 10:957–959
Vysotskii GN (1905) Gley, Pochvovedenie no. 4
Walkley A, Black IA (1934) An examination of Degtjareff method for determining soil organic matter and a proposed modification of the chromic acid titration method. Soil Sci 37:29–37
Zaidelman FR, Nikiforova AS (1994) Genesis and Diagnostic Value of Neoformations in Soils of the Forest and Forest-Steppe Zone (Moscow, 2001) [in Russian]
Zhang YL, Evangelou VP (1996) Influence of iron oxide forming conditions on pyrite oxidation. Soil Sci 161:852–864